01 Dec 2010

Feedback Control of a Bioinspired Plate-Beam System

Cody W. Ray

Belinda A. Batten

John R. Singler
Missouri University of Science and Technology, singlerj@mst.edu

Recommended Citation

C. W. Ray et al., "Feedback Control of a Bioinspired Plate-Beam System," *Proceedings of the 49th IEEE Conference on Decision and Control (2010, Atlanta, GA)*, Institute of Electrical and Electronics Engineers (IEEE), Dec 2010.
The definitive version is available at https://doi.org/10.1109/CDC.2010.5717811

Feedback Control of a Bioinspired Plate-Beam System

Cody W. Ray and Belinda A. Batten
School of Mechanical, Industrial,
& Manufacturing Engineering
Oregon State University
Corvallis, Oregon 97331-6011
Email: raycod@onid.orst.edu
bbatten@engr.orst.edu

John R. Singler
Department of Mathematics
& Statistics
Missouri University of Science & Technology
Rolla, Missouri 65409-0020
Email: singlerj@mst.edu

***Abstract*—In this paper we present a model for a plate-beam system to represent a bioinspired flexible wing. Using a Galerkin based finite element approximation to the system, we compute functional gains that can be used for sensor placement and show that a piezoceramic actuator on the beam can be used for camber control.**

I. Introduction

Increasing interest in deploying micro aerial vehicles (MAVs) in a variety of complex scenarios motivates equipping them with a variety of capabilities not currently in the design suite. These capabilities include flying in cluttered and unpredictable urban environments, through forests and buildings, and in poor weather. While some MAVs have limited success in these flight situations, they are lacking overall situational awareness and many of the behaviors readily observed in biological fliers. Our group has been part of a multi-disciplinary team researching bat flight and the behaviors that might be leveraged to increase MAV agility and maneuverability. In this paper we describe the first step of a closed-loop analysis of how bats control camber in their wings to increase lift, decrease drag or simply accommodate aerodynamic changes.

Our long range goal is to construct a closed loop system of the membrane wing with smart actuators to simulate muscles in the bat and hair cell sensors studied extensively by Dickinson [1]–[3] to sense flow over the wing. The overall aerodynamic properties under a variety of flow conditions would be studied, particularly how changes in camber affect flight performance. In this paper, we present the membrane beam model with piezoceramic actuation over the beam, and consider the closed loop performance of the system in response to prescribed initial conditions and external forcing.

A. Model Derivation

The bat wing is composed of an anisotropic membrane surface (skin) stretched over a network of bones with muscles to control flapping and maintain tension during flight (see Figure 1(a)). We begin with a model of a wing segment constructed of a rectangular membrane, rigid on two sides, with a beam on the third and a free end at the fourth (see Figure 1(b)). We interpret the rigidity of the two sides to represent the leading edge and attachment to the body. The beam has a piezoceramic actuator attached, which will be used to affect camber control. The free edge replicates the trailing edge of the wing. While the membrane-like material of the bat wing does not lend itself readily to thin plate theory, we hypothesize that at least some of the important aspects of the aerodynamic performance of bat flight can be accounted for by thin plate theory, without necessitating the use of nonlinear plate/membrane theory. Such aspects include steady state camber changes. For the purposes of this study,

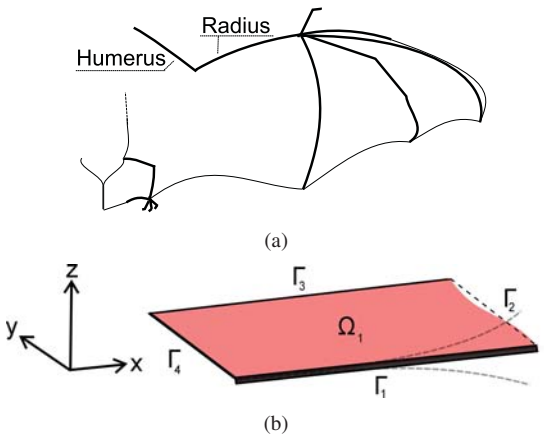

Fig. 1. Bat wing schematic (top) and side view of plate-beam system (bottom)

we derived the equations modeling a thin, orthotropic plate. An orthotropic plate was chosen to more accurately model the anisotropic bat wing membrane, which varies up to 1000:1 in spanwise vs chordwise stiffness [4]. For this paper, an orthotropic plate made of a rubber-like material was chosen (see table I).

Detailed derivations of the model of an orthotropic plate can be found in a variety of textbooks on thin plate theory such as [5]. Following standard stress analysis methodology, balancing moment and shear forces, we obtain the standard

orthotropic plate model:

$$\begin{aligned}\rho_p h w_{tt} + \left[D_{E_x}\left(w_{xx} + \nu_2 w_{yy}\right)\right]_{xx} \\ + \left[D_{E_y}\left(w_{yy} + \nu_1 w_{xx}\right)\right]_{yy} + 2\left[K_E w_{xy}\right]_{yx} \\ + 2\left[K_E w_{yx}\right]_{xy} + \left[D_{\beta_1}(w_{txx} + \nu_2 w_{tyy})\right]_{xx} \\ + \left[D_{\beta_2}(w_{tyy} + \nu_1 w_{txx})\right]_{yy} + 2\left[K_\beta w_{txy}\right]_{yx} \\ + 2\left[K_\beta w_{tyx}\right]_{xy} + \gamma w_t = f(t,x,y) \qquad (1)\end{aligned}$$

where $f(t,x,y)$ is an external forcing function. We have suppressed (x,y) dependence on the parameters above which are defined as follows:

$$\begin{aligned} D_{E_x}(x,y) &= \frac{E_x(x,y)\, h_p^3(x,y)}{12(1-\nu_1(x,y)\nu_2(x,y))} \\ D_{E_y}(x,y) &= \frac{E_y(x,y)\, h_p^3(x,y)}{12(1-\nu_1(x,y)\nu_2(x,y))} \\ D_{\beta_{1,2}}(x,y) &= \frac{\beta_{1,2}(x,y)\, h_p^3(x,y)}{12(1-\nu_1(x,y)\nu_2(x,y))} \\ K_E(x,y) &= \frac{G_D\, h_p^3}{12} \\ K_\beta(x,y) &= \frac{G_\beta\, h_p^3}{12} \\ G_D(x,y) &= \frac{E_x(x,y)}{2(1+\nu_1(x,y))} \\ G_\beta(x,y) &= \frac{\beta_1(x,y)}{2(1+\nu_1(x,y))}. \end{aligned}$$

The parameter contributions due to the patch are calculated using formulas found in [6]. The formula used for patch contributions to beam stiffness is

$$EI(x) = \frac{E_b W_b h_b^3}{12} + E_p W_{pz}\left[h_b T^2 + \frac{1}{2}h_b^2 T + \frac{2}{3}T^3\right] H(x).$$

Other patch contributions are calculated similarly.

The plate is attached to the beam on boundary Γ_1 (see Figure 1(b)) through interface conditions formed by balancing the relevant shear force. It is assumed that the beam does not support torsion and , therefore, no moment balancing is necessary along boundary Γ_1. These assumptions yield the following dynamic boundary condition

$$\begin{aligned}&\rho_b v_{tt}(t,x) + \left[\beta_b I v_{txx}(t,x) + EI\, v_{xx}(t,x)\right]_{xx} \\ &= \Big\{\left[D_{E_y} w_{yy} + \nu_1\, w_{xx}\right]_y + 2\left[K_E w_{xy}\right]_x + 2\left[K_E w_{yx}\right]_x \\ &\qquad + \left[D_{\beta_2}[w_{tyy} + \nu_1 w_{txx}]\right]_y + 2\left[K_\beta w_{txy}\right]_x \\ &\qquad + 2\left[K_\beta w_{tyx}\right]_x\Big\}\Big|_{y=0} + \left[\kappa(H_1 - H_2)\right]_{xx} u(t). \qquad (2)\end{aligned}$$

The last term in equation (2) represents the control input to the system consisting of applied voltage, $u(t)$, coefficient for piezoceramic material, $\kappa = E_p d_{31}(h_b + T)$ and Heaviside functions $H_1 = H(x_1)$, $H_2 = H(x_2)$, where x_1, x_2 indicates the location of the beginning and end of the piezoceramic patch as mounted on the beam.

There is a free edge on the plate at boundary Γ_2 with conditions that state there is no shear force

$$\begin{aligned}\Big\{&\left[D_{E_1}[w_{xx} + \nu_2 w_{yy}]\right]_x + 2\left[K_E\, w_{yx}\right]_y \\ &+2\left[K_E\, w_{xy}\right]_y + \left[D_{\beta_1}[w_{txx} + \nu_2 w_{tyy}]\right]_x \\ &+2\left[K_\beta\, w_{tyx}\right]_y + 2\left[K_\beta\, w_{txy}\right]_x\Big\}\Big|_{\Gamma_2} = 0\end{aligned}$$

and no moment about the y-axis,

$$\left\{D_{E_1}[w_{xx} + \nu_2 w_{yy}] + D_{\beta_1}[w_{txx} + \nu_2 w_{tyy}]\right\}\Big|_{\Gamma_2} = 0.$$

The boundary conditions for the beam include no shear force at the tip,

$$\left[\beta_b I v_{txx} + EI v_{xx}\right]_x\Big|_{x=L} = 0,$$

and no bending moment,

$$\left[\beta_b I v_{txx} + EI v_{xx}\right]\Big|_{x=L} = 0.$$

On boundary Γ_3, the plate is clamped. This is stated mathematically as both the vertical deflection and the derivative in the normal direction being identically zero,

$$w\Big|_{\Gamma_3} = 0, \qquad w_y\Big|_{\Gamma_3} = 0.$$

On boundary Γ_4, the plate is also clamped, so

$$w\Big|_{\Gamma_4} = 0, \qquad w_x\Big|_{\Gamma_4} = 0.$$

Similarly, for the beam, we have clamped boundary conditions at the root,

$$v\Big|_{\Gamma_4} = 0, \qquad v_x\Big|_{\Gamma_4} = 0.$$

Finally, at the corners of the system in Figure 1(b) in which a clamped and free edge meet ((Γ_4,Γ_1), (Γ_2,Γ_3)), or free edges meet (Γ_1,Γ_2), there must be zero bending moment. These corner boundary conditions are summarized as:

$$\begin{aligned}\left(2K_E\, w_{yx} + 2K_\beta\, w_{txy}\right)\Big|_{(x,y=0)} &= 0 \\ \left(2K_E\, w_{yx} + 2K_\beta\, w_{txy}\right)\Big|_{(x=L,y=W)} &= 0 \\ \left(2K_E\, w_{yx} + 2K_\beta\, w_{txy}\right)\Big|_{(x=L,y=0)} &= 0.\end{aligned}$$

Multiplying both the plate and beam equations (1) and (2) by test functions $\phi(x)$ and $\psi(x)$ respectively, and integrating by parts (or applying the divergence theorem in component form found in [7]), we arrive at the weak form of the beam and plate equations. After application of relevant boundary conditions, adding the weak forms of both partial differential equations and defining $\phi(x,0) = \psi(x)$ on Γ_1, several terms

cancel, leaving

$$\begin{aligned}
&\int_{\Omega} (\rho_1 h w_{tt} + \gamma w_t)\phi \\
&+ \left[D_{E_1}\left(w_{xx} + \nu_2 w_{yy}\right) + D_{\beta_1}\left(w_{txx} + \nu_2 w_{tyy}\right)\right]\phi_{xx} \\
&+ \left[D_{E_2}\left(w_{yy} + \nu_1 w_{xx}\right) + D_{\beta_2}\left(w_{tyy} + \nu_2 w_{txx}\right)\right]\phi_{yy} \\
&\qquad + 2\left[K_E w_{yx} + K_\beta w_{tyx}\right]\phi_{yx} \\
&\qquad + 2\left[K_E w_{xy} + K_\beta w_{txy}\right]\phi_{xy} d\Omega \\
&\quad + \int_{\Gamma_1} \left\{\rho_2 A v_{tt}\phi + \left[\beta_b I v_{txx} + EI v_{xx}\right]\phi_{xx}\right\} dx \\
&= \int_{\Omega_1} f(t,x,y)\phi d\Omega + \int_{\Gamma_1} \kappa\left[H_1 - H_2\right] u(t)\phi_{xx} dx. \qquad (3)
\end{aligned}$$

Equation (3) shows that, due to the nature of the models used for the plate and beam, the full system simplifies to a plate model with parameter adjustments along one edge, with the additional requirement of zero slope in the normal direction. This condition is required because the beam model used here does not support torsion.

II. Finite Element Approximation

To form the Galerkin finite element approximation for this system, we make the substitution

$$w(t,x,y) \approx \sum_{i=1}^{N} z_i(t)\,\phi_i(x,y)$$

into the weak form of the system in equation (3). We choose the shape functions ϕ to be bicubic B-splines on a rectangular mesh. Given the connection between the beam and plate, we have

$$v(t,x) = w(t,x,0) \approx \sum_{i=1}^{N} z_i(t)\,\phi_i(x,0).$$

Substituting these terms into equation (3) and simplifying through linear algebra yields the matrix approximation to the plate-beam system

$$M\ddot{z} + D\dot{z} + Kz = B_0 u(t) + F_0(t),$$

where dots are used to indicate differentiation in time. These matrix approximations are composed of

$$\begin{aligned}
M &= [M_1] + [M_b] \\
K &= [K_1] + [K_2] + [K_3] + [K_4] + [K_b] \\
D &= [C_1] + [C_2] + [C_3] + [C_4] + [C_5] + [C_b]
\end{aligned}$$

where the individual matrices are defined as

$$\begin{aligned}
[M_1]_{i,j=1}^{N} &= \int_{\Omega_1} \rho_1 h \phi_i \phi_j d\Omega \\
[K_1]_{i,j=1}^{N} &= \int_{\Omega_1} D_{E_1}\left(\left[\phi_i\right]_{xx} + \nu_2\left[\phi_i\right]_{yy}\right)\left[\phi_j\right]_{xx} d\Omega \\
[K_2]_{i,j=1}^{N} &= \int_{\Omega_1} D_{E_2}\left(\left[\phi_i\right]_{yy} + \nu_1\left[\phi_i\right]_{xx}\right)\left[\phi_j\right]_{yy} d\Omega \\
[K_3]_{i,j=1}^{N} &= \int_{\Omega_1} 2K_E\left[\phi_i\right]_{yx}\left[\phi_j\right]_{yx} d\Omega \\
[K_4]_{i,j=1}^{N} &= \int_{\Omega_1} 2K_E\left[\phi_i\right]_{xy}\left[\phi_j\right]_{xy} d\Omega \\
[C_1]_{i,j=1}^{N} &= \int_{\Omega_1} D_{\beta_1}\left(\left[\phi_i\right]_{xx} + \nu_2\left[\phi_i\right]_{yy}\right)\left[\phi_j\right]_{xx} d\Omega \\
[C_2]_{i,j=1}^{N} &= \int_{\Omega_1} D_{\beta_2}\left(\left[\phi_i\right]_{yy} + \nu_1\left[\phi_i\right]_{xx}\right)\left[\phi_j\right]_{yy} d\Omega \\
[C_3]_{i,j=1}^{N} &= \int_{\Omega_1} 2K_\beta\left[\phi_i\right]_{yx}\left[\phi_j\right]_{yx} d\Omega \\
[C_4]_{i,j=1}^{N} &= \int_{\Omega_1} 2K_\beta\left[\phi_i\right]_{xy}\left[\phi_j\right]_{xy} d\Omega \\
[C_5]_{i,j=1}^{N} &= \int_{\Omega_1} \gamma\phi_i\phi_j d\Omega \\
[M_b]_{i,j=1}^{N} &= \int_{\Gamma_1} \rho_2 A\phi_i(x,0)\phi_j(x,0) dx \\
[C_b]_{i,j=1}^{N} &= \int_{\Gamma_1} \beta_b I\left[\phi_i(x,0)\right]_{xx}\left[\phi_j(x,0)\right]_{xx} dx \\
[K_b]_{i,j=1}^{N} &= \int_{\Gamma_1} EI\left[\phi_i(x,0)\right]_{xx}\left[\phi_j(x,0)\right]_{xx} dx \\
[F_0]_{j}^{N} &= \int_{\Omega_1} f\phi_i dx \\
[B_0]_{j}^{N} &= \int_{\Gamma_1} k\left[H_1 - H_2\right]\phi_{xx} dx.
\end{aligned}$$

For simulation and control purposes, we write this system in first order state space form with initial conditions as

$$\dot{z} = Az + Bu(t) + F(t), z(0) = z_0, \qquad (4)$$

where

$$A = \begin{bmatrix} 0 & I \\ -M^{-1}K & -M^{-1}D \end{bmatrix} \qquad (5)$$

$$B = \begin{bmatrix} 0 \\ M^{-1}B_0 \end{bmatrix} \qquad F = \begin{bmatrix} 0 \\ M^{-1}F_0 \end{bmatrix}. \qquad (6)$$

III. Control Methodology

We begin with the model in equations (4) - (6)

$$\dot{z} = Az + Bu(t) + F(t), z(0) = z_0.$$

Making the substitution $x = z - z_d$, where z_d is the desired function to track, we obtain

$$\begin{aligned}
\dot{x} &= Ax + Bu(t) + F(t) + (Az_d - \dot{z}_d), \\
x(0) &= z(0) - z_d(0).
\end{aligned}$$

Since matrix A and functions z_d and $\dot{z}_d$ are known, the problem then becomes one of driving the tracking error x to zero. Thus the problem statement is summarized as: given

the known disturbance $d(t)$, find the control $u^*(t)$ such that $u^* = \min_u J(u)$, where

$$J = \int_0^{t_f} x^T Q x + u^T R u dt,$$

subject to the constraints

$$\begin{aligned} \dot{x} &= Ax + Bu + F(t) + d \\ d &= Az_d - \dot{z_d} \\ x(0) &= z(0) - z_d(0). \end{aligned}$$

The Differential Ricatti Equation (DRE) and a differential equation for feed forward function b must be solved to obtain the optimal control law $u(t)$,

$$-\dot{\Pi} = \Pi A + A^T \Pi - \Pi B R^{-1} B^T \Pi + Q \quad (7)$$

$$\dot{b} = -\left(A^T - \Pi B R^{-1} B^T\right) b - \Pi d. \quad (8)$$

Equation (7) is the general solution for $\Pi(t)$. Setting $\dot{\Pi} = 0$ yields the *steady state regulator* problem, in which the optimization time interval is infinite; this process yields the algebraic Ricatti equation (ARE),

$$0 = \bar{\Pi} A + A^T \bar{\Pi} - \bar{\Pi} B R^{-1} B^T \bar{\Pi} + Q,$$

where $\bar{\Pi}$ denotes the steady state solution for $\Pi(t)$. Thus the control problem for the finite element system is written

$$\begin{aligned} \dot{x}(t) &= Ax(t) + Bu(t) + F(t) + d(t) \\ d(t) &= Az_d(t) - \dot{z_d}(t) \\ u(t) &= -R^{-1} B^T \bar{\Pi} x(t) - R^{-1} B^T b(t), \end{aligned}$$

where $b(t)$ is the solution to equation (III).

IV. Numerical Results

Functional gains for two scenarios and one set of simulations are presented here to demonstrate the control effectiveness of a piezoceramic in camber control. A discussion of functional gains can be found in [6], [8]–[10]. The patch itself was assumed to be bonded perfectly to the beam, and extends from $x_1 = .15\text{m}$ to $x_2 = .35\text{m}$ such that the ends of the patch align with the finite element nodes for even element numbers. A mesh consisting of N nodes in the x and y directions yields $2N^2 - 2N$ states in the system. Three meshes were used in the numerical experiments to test convergence of the results, corresponding to $N = 8, 16, 32$ elements in each direction. The simulations were obtained using the ODE23s stiff system Runge-Kutta integration routine in Matlab. Parameters used in this study are summarized in Table I and were held constant for all simulations. Patch parameters were taken from [11].

A. Control Gains and Convergence

In all computations, $R = 1e^{-2}$ was used. Control functional gains were calculated using the equation

$$[k_b \; k_v]^T = \begin{bmatrix} K & 0 \\ 0 & M \end{bmatrix}^{-1} K_c^T, \quad (9)$$

where k_b and k_b are the bending and velocity gains, respectively, and $K_c = R^{-1} B^T \bar{\Pi}$. To compute control functional gains, two choices for the state weight Q were used. The first,

$$Q = \begin{bmatrix} q_1 K_b & 0 \\ 0 & q_2 M_b \end{bmatrix}, \quad (10)$$

with $q_1 = 1 \times 10^6$ and $q_2 = 1$, was chosen to focus control effort on the beam as a controlled output. One would expect that the camber of the beam would be more closely controlled in this scenario.

Convergence of the bending and velocity gains was verified. In Figures 2(a)-2(b) the gains are plotted for aforementioned 32×32 element computation. These gains bear similarity to those found in literature, including [6]. Notice the location of the dominant features of the plots coincides with the location of the patch. As the number of elements gets larger, the surface plot features tend to the edge of the plate, becoming less two dimensional in support, and along the beam, more closely resembling those of a stand-alone beam-patch combination.

The second choice of state weight Q corresponds to the identity weighting or

$$Q = \begin{bmatrix} q_1 K & 0 \\ 0 & q_2 M \end{bmatrix}, \quad (11)$$

where again, $q_1 = 1 \times 10^6$ and $q_2 = 1$. Defining the Q matrix in terms of the global stiffness and mass matrices results in functional gains with support generally in the same location along the beam, but with different shapes (see Figures 3(a) - 3(b)). For the locally defined Q weight in equation (10), there is a peak at the free corner for the bending gain, which indicates strong sensitivity to strain at that location. This effect is even more pronounced in the second case for Q in equation (11) where the states are identically weighted. Notice the surface features located where free and clamped edges meet. These features are similar to those expected by basic stress analysis theory.

TABLE I
Material Parameters

	Plate	Beam	Patch
$L(m)$	.4	.4	.2
$W_{p,b}(m)$	.4	.0125	.0125
$h_{p,b}(m)$	.0005	.001	.002
$E_x(GPa)$	1.0	23	28.6
$E_y(GPa)$	0.1	n/a	n/a
ν_x, ν_y	.3	n/a	n/a
$\beta_{1,2}(N\,m\,s) \times 10^{-4}$	1.29	1.29	.896
$\rho_p(kg/m^3) \times 10^6$	1	1.4	5.3
$T(m)$	n/a	n/a	.003
$d_{31}(m/v) \times 10^{-12}$	n/a	n/a	290

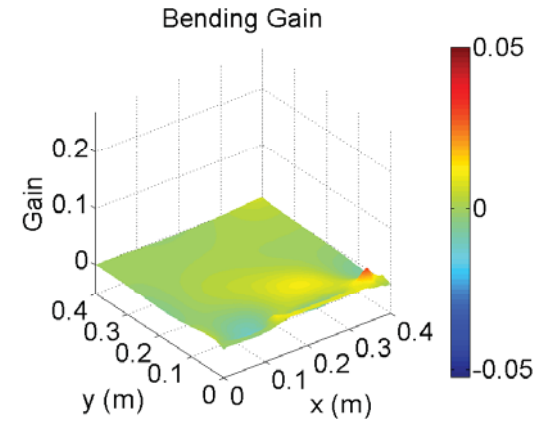

(a)

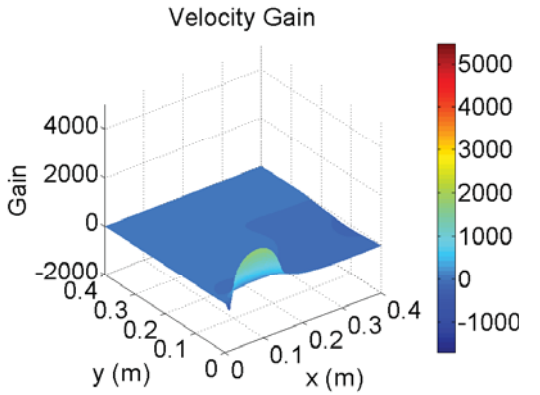

(b)

Fig. 2. Bending gain on plate (top), and velocity gain on plate (bottom

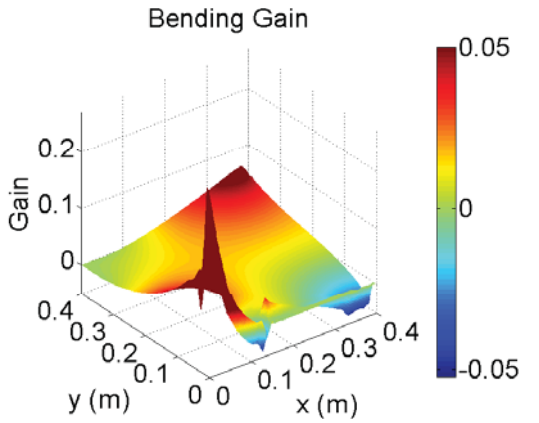

(a)

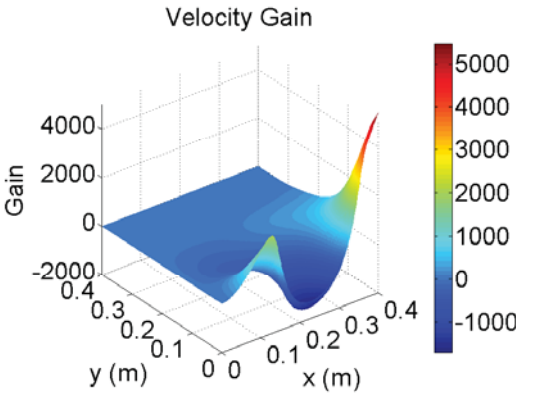

(b)

Fig. 3. Bending gain on plate (top), and velocity gain on plate (bottom)

Results such as these will be used to place sensors for the closed loop investigations of camber control, e.g. [8] and [9].

B. Tracking with External Forcing

To test the efficacy of a piezoceramic patch on a beam to control camber in the presence of an external forcing function, we used the desired shape function as defined by the first mode shape of the beam multiplied by $W_p - y$ to interpolate across the domain Ω

$$z_d = \frac{(W_p - y)}{128}(\cosh(\alpha x) - \cos(\alpha x) - \sigma(\sinh(\alpha x) - \sin(\alpha x)))$$

where $\alpha = 1.8751040/L$, $\sigma = 0.7341$. We then repeated the process for the y direction, and multiplied these together with an appropriate constant to achieve the desired state illustrated as a blue surface in Figure 5(a). The external forcing is given by

$$F(t) = (\cos(25\pi t) + \cos(50\pi t) + \sin(90\pi t))\, F_0,$$

where F_0 is defined in equation 4. The force is not homogeneously distributed over the plate, rather it is distributed using the desired state function, so that the maximum force occurs at the free corner and zero force occurs along the clamped edges. The first case of the state weighting matrix where the beam is the controlled output was used.

We see in Figures 4(a) - 5(b) that the voltage applied to the patch to maintain the desired position is at the realistic limit. While these results show that camber control of the overall system position with a piezoceramic is acceptable, there is a residual vibration (easily seen in the beam tip plot). This is not unexpected given the choice of state weight, use of a single actuator and the external force disturbance. A greater number of actuators may enhance the tracking capabilities of this system.

V. Conclusion and Future Directions

In this work, we showed that a piezoceramic patch along a single edge of a plate can be used for steady state control problems related to wing morphing and camber. We computed two sets of control functional gains corresponding to bending and velocity; results such as these can and will be used for sensor placement. We demonstrated a steady state tracking problem indicative of a wing maintaining a certain camber during flight. This problem was solved in the presence of an external periodic force.

There are drawbacks to using piezoceramics as actuators for MAVs, the most notable of which is their very low control authority. Placement of more patches will alleviate this issue, as will the utilization of more flexible materials. The value of

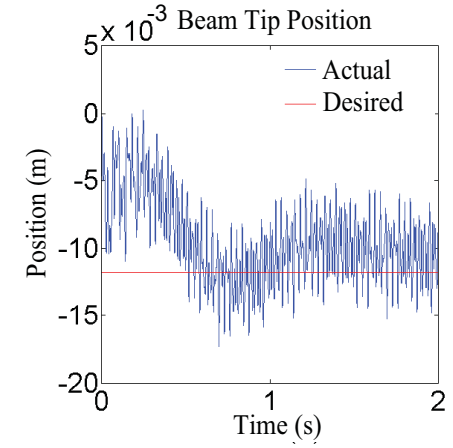

(a)

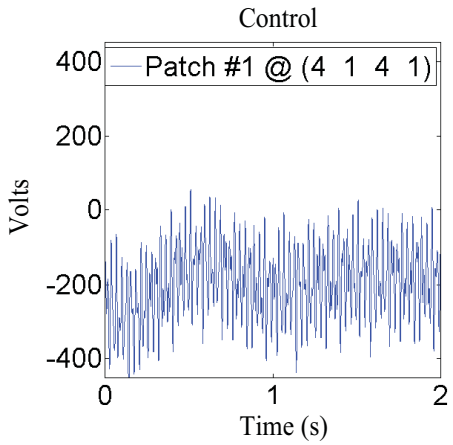

(b)

Fig. 4. Beam tip position in time (top), and control applied (bottom)

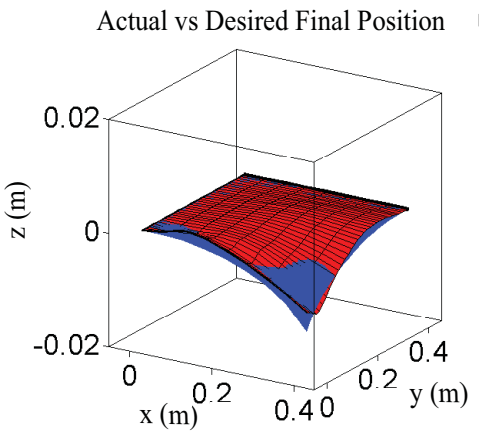

(a)

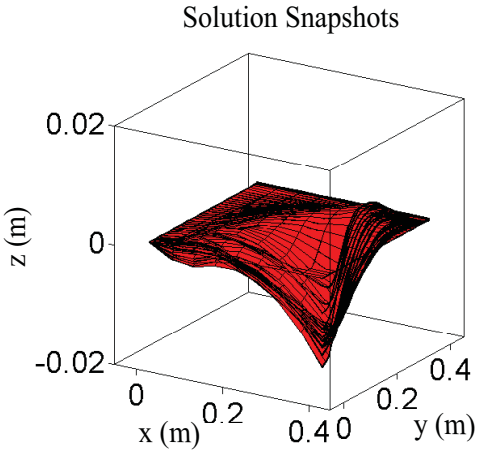

(b)

Fig. 5. Final and desired plate position (top), and solution snapshots (bottom)

the control authority coefficient, R, could also be adjusted to maximize the potential of the piezoceramic device.

Immediate future work will include the utilization of more patches in the domain to increase control authority, inclusion of sensors and an estimator design, and potentially a physically more meaningful external disturbance. Throughout all of these adaptations to the work, sensor placement will be studied using control gains. This work will culminate with the use of real fluid flow simulation data, as well as the full fluid structure interaction problem.

ACKNOWLEDGMENT

This work was supported in part by the Air Force Office of Scientific Research under the Multidisciplinary University Research Initiative grant FA9550-07-1-0540.

REFERENCES

[1] B. Dickinson, J. Singler, and B. A. Batten, "Modeling of bioinspired sensors for flow separation detection in micro air vehicles," *Proceedings of the 3rd AIAA Flow Control Conference*, no. AIAA paper 2006-3019, 2006.

[2] B. Dickinson, J. Singler, and B. Batten, "The detection of unsteady flow separation with bioinspired hair cell sensors," in *26th AIAA Aerodynamic Measurement Technology and Ground Testing Conference*, no. 2008-3937. American Institute of Aeronautics and Astronautics AIAA, 2008.

[3] B. Dickinson, "Hair receptor sensitivity to changes in laminar boundary layer shape," *Bioinspiration & Biomimetics*, vol. 5, p. 11, 2010.

[4] S. Swartz, "Skin and bones: The mechanical properties of bat wing tissues," *Bats: Phylogeny, Morphology, Echolocation, and Conservation Biology*, pp. 109–126, 1998.

[5] A. Ugural, *Stresses in Plates and Shells*, 2nd ed. McGraw -Hill, 1999.

[6] H. Banks, K. Ito, and B. King, "Theoretical and computational aspects of feedback in structural systems with piezoceramic controllers," in *Computation and Control III*, K. Bowers and J. Lund, Eds., Progress in Systems and Control theory. Birkhauser, 1992.

[7] M. Gockenbach, *Understanding and Implementing the Finite Element Method*. Society for Industrial and Applied Mathematics (SIAM), 2006.

[8] J. Burns and B. King, "Optimal sensor location for robust control of distributed parameter systems," *Proceedings of the 33rd Conference on Decision and Control*, pp. 3967 – 3972, 1994.

[9] A. Faulds and B. King, "Sensor location in feedback control of partial differential equation systems," *Proceedings of the 2000 IEEE International Conference on Control Applications*, pp. 536 – 541, 2000.

[10] E. Ruggiero, "Modeling and control of spider satellite components," Ph.D. dissertation, Virginia Polytechnic Institute and State University, 2005.

[11] H. Banks, R. Smith, and Y. Wang, *Smart Material Structures: Modeling, Estimation and Control*, P. Ciarlet and J.-L. Lions, Eds. John Wiley & Sons, 1996.